An optical H2S biosensor based on the chemoselective Hb-I protein tethered to a transparent, high surface area nanocolumnar electrode

Martin Dulac, Armelle Melet, Kenneth R. Harris, Benoit Limoges, Erwan Galardon, Véronique Balland

An optical H_2S biosensor based on the chemoselective Hb-I protein tethered to a transparent, high surface area nanocolumnar electrode

Martin Dulac,[1,2] Armelle Melet,[1] Kenneth D. Harris,[3] Benoît Limoges,[2] Erwan Galardon[,1] & Véronique Balland[*,2]*

1- Laboratoire de Chimie et Biochimie Pharmacologiques et Toxicologiques, UMR CNRS 8601, Université Paris Descartes, Sorbonne Paris Cité, 45 rue des Saints Pères, F-75270 Paris Cedex 06

2- Laboratoire d'Electrochimie Moléculaire, UMR CNS 7591, Université Paris Diderot, Sorbonne Paris Cité, 15 rue J-A de Baïf, F-75205 Paris Cedex 13

3- National Research Council Canada, Nanotechnology Research Center, Edmonton, Alberta T6G 2M9, Canada & Department of Mechanical Engineering, University of Alberta, Edmonton, Alberta T6G 2V4, Canada

Corresponding Author *veronique.balland@univ-paris-diderot.fr

.

ABSTRACT

Sensitive and selective detection of analytes in complex biological fluids can be an extremely challenging issue. The constructive association of biomolecules and transparent mesoporous electrodes is of interest in this area, as it can lead to innovative biosensors combining optical and electrochemical detection modes. This concept, however, requires the development of appropriate surface functionalization methodologies that are robust enough for long-term operation in physiological environments. In the present work, the high-surface area of 3D transparent mesoporous indium-tin oxide (ITO) electrodes (prepared by glancing angle deposition or GLAD) has been chemically functionalized with recombinant hemoglobin I from *Lucina pectinata* according to a versatile 2-step process. First, 4-diazoniumbenzoic acid salt is covalently electrografted onto the ITO surface, followed by amide coupling of the protein. The resulting electrodes were quantitatively characterized by cyclic voltammetry and UV-visible absorption spectroscopy, demonstrating high surface coverages (up to 45% of a closed-packed monolayer for Hemoglobin-I) and homogeneous distribution across the entire thickness of the GLAD mesoporous structure. Good stability is also observed when the modified electrodes are immersed for prolonged times in a high ionic strength saline buffer. We also show that the hemoglobin I-modified electrode can be used as an optical biosensor for the selective, reversible, and fast detection of H_2S in aqueous solutions over a ~two-decade concentration range and with a limit of detection of 0.35 μM. Good analytical performance was also achieved in human plasma without significant interference from the biological matrix.

KEYWORDS: diazonium electrografting; metal oxide electrodes; glancing angle deposition; biosensors; hemoglobin-I; hydrogen sulfide.

1. Introduction

Mesoporous conductive electrodes (meso-TCEs) based on wide band-gap doped metal oxide films such as indium tin oxide (ITO) or antimony-doped tin oxide (ATO) are characterized by optical transparency in the visible range, good electrical conductivity and large surface area. These properties allow meso-TCEs to be used to develop sensitive biosensors; the large surface area allows the immobilization of huge amounts of bioreceptor per unit of geometric electrode area, and because meso-TCEs are transparent and electrically conducting, both optical and electrochemical detection modes can be integrated into the same device.[1] In some cases, these strategies can be extremely helpful for reliably detecting molecules in complex biological media.[2]

The development of such innovative biosensing devices based on the constructive association of bioreceptors (e.g., proteins, enzymes, DNA, ...) and meso-TCEs requires overcoming a number of challenges. First, the nanostructured metal oxide film must be fabricated with stringent reproducibility, including a well-defined accessible porosity and a highly controlled morphology. A second challenge is the preparation of reproducible and highly stable surface-functionality, allowing reliable and long-lasting operation of the biosensing surface under physiologically-relevant conditions.

In the present study, highly reproducible nanostructured ITO electrodes are used as 3D transparent conductive surfaces for the immobilization of a protein-based bioreceptor. These transparent 3D electrodes were obtained by glancing angle deposition (GLAD),[3] a physical vapor deposition technique that allows for the production of highly reproducible nanocolumnar films with an accessible pore structure.[4] We have previously shown that GLAD-ITO electrodes are particularly well suited for the immobilization of small hemoproteins through simple

physisorption, allowing real-time spectroelectrochemical characterization.[5,6] In these studies, however, low ionic strength conditions were required in order to minimize protein desorption resulting from insufficient protein/metal oxide anchoring. In order to improve the binding of protein to the GLAD-ITO electrode, we propose here to covalently attach the biomolecule onto the ITO surface through a multi-step covalent surface functionalization. To date, only a few studies report on such immobilization strategies within meso-TCE electrodes.[7–10] Moreover, these studies rely on the pre-functionalization of the meso-TCE with amino- or carboxylate moieties through either chemisorbed phosphonic acids [7] or surface-condensed organosilanes [8][9,10], two surface functionalization strategies that are not recognized for their high stability in aqueous media. A better alternative, which has recently emerged in the literature for the surface-functionalization of meso-TCEs, is to take advantage of the covalent electrochemical grafting of aryl-diazonium salts.[11–13] This method is highly versatile, simple, efficient and able to operate with a wide range of metal oxide surfaces. Also, because this is an electrodeposition approach, it offers the additional advantage of reliably grafting molecules on conductive surfaces, regardless of their shapes and porosities. The method was successfully applied to the robust surface modification of meso-TCE electrodes with redox active dyes, leading to improved stability under hydrolytic aqueous conditions as compared to other surface functionalization chemistries.[11–13]

Herein, we prepare robust GLAD-ITO electrodes pre-functionalized with carboxylate moieties through the electrochemical reduction of aryl diazonium salts. The resulting pre-functionalized electrodes are then used as a versatile platform for further covalent immobilization of the bioreceptor hemoglobin I from *Lucina pectinata.* Similar 2-step functionalization methods have previously been used to modify planar carbon and gold electrodes with biomolecules [14–16],

however, the application of these methods to mesoporous metal-oxide electrodes remains challenging because the composition, porosity and high surface area of the meso-TCEs have an unknown effect over the homogeneity, reproducibility and stability of the modified electrodes, especially for the covalent immobilization of macrobiomolecules which haven't previously been explored. These issues are addressed in the present study.

To be suitable for the development of opto-electronic biosensors, the first functionalization step must preserve the electrode transparency as well as the interfacial electron transfer properties. We therefore selected 4-aminobenzoic acid as it is commercially available and easy to convert to its diazonium salt. The resulting electrografted electrodes were then further functionalized with two different probes (see Scheme 1) to optimize the coupling procedures and to study the influence of the amide-coupling over the reactivity of the modified electrode. We thus used aminoferrocene (Fc-NH_2), a small reversible one-electron oxidation probe useful for quantitative electrochemical characterization of the functionalized electrodes,[17] and 5,10,15,20-tetrakis(4-aminophenyl)porphyrin (TAPP) as an optical probe enabling characterization by UV-visible absorption spectroscopy. Finally, we considered the development of a functional biosensor targeting the analyte H_2S, which has recently been recognized for its importance in cell signaling and proposed as a potential therapeutic target for inflammatory diseases.[18,19] Moreover, the bioavailability of H_2S in Caucasian male plasma has been validated as predictive for cardiovascular disease,[20] clearly calling for development of analytical tools for its real-time detection under physiological conditions. Only a few H_2S biosensors have been reported to date, and they are all based on the ability of H_2S to inhibit enzymatic systems such as cytochrome c oxidase, peroxidases or ascorbate oxidase.[21] These systems are unlikely to meet the requirements for application in a biological setting because of

their low selectivity towards other inhibitors and sulfur-containing biomolecules. We anticipate that the recombinant protein Hemoglobin I from the clam *Lucina pectinata* (rN6KHbI) would be a much better H_2S bioreceptor because of its rapid, selective, highly affine and reversible binding to H_2S.[22,23] H_2S coordination at the heme of rN6KHbI induces a transition from high spin met-aquo form to low spin met-sulfide accompanied by significant modifications of the spectroscopic features of the protein.[24,25] We studied this transition for optical H_2S-biosensing in both buffer solutions and human plasma.

2. Experimental section

Materials. HEPES (≥ 99.5%), HEPES sodium salt (≥ 99.5%), 2-(N-morpholino)ethanesulfonic acid hydrate (MES, ≥ 99.5%), MES sodium salt (≥ 99%), 4-aminobenzoic acid (98%) and $NaNO_2$ were purchased from Sigma-Aldrich. Aminoferrocene (Fc-NH_2, > 96%) and KCl were obtained from TCI and Merck, respectively. N-hydroxysuccinimide (NHS ≥ 97%) was provided by FLUKA, and 1-(3-dimethylaminopropyl)-3-ethylcarbodiimide hydrochloride (EDC, + 98%) and anhydrous Na_2S were obtained from Alfa Aesar. HCl (37%) was purchased from VWR and 5,10,15,20-tetrakis(4-aminophenyl)porphyrin from Porphychem. Aqueous solutions were all prepared using ultrapure water (18.2 MΩ·cm). The planar indium tin oxide coated glass substrates (8-12 Ω/□) used to support the GLAD-ITO and 2D-ITO electrodes were purchased from Delta Technologies and Sigma-Aldrich , respectively.

Electrode preparation. Mesoporous GLAD-ITO electrodes were prepared according to the previously published procedure.[4,26] Briefly, electron beam evaporation was used to deposit ITO on flat ITO/glass substrates positioned at a highly oblique deposition angle of 80°. The substrates were continuously rotated during deposition at a rate of one complete rotation for

every 10 nm of ITO film growth. A series of mesoporous ITO films with thicknesses ranging from 0.3 μm to 2 μm was obtained by varying the duration of the glancing angle deposition process. The GLAD-ITO electrodes were then subjected to two successive thermal annealing steps (air at 500°C followed by forming gas at 375°C) in order to increase the film transparency and conductivity. For such deposition conditions, an electroactive surface enhancement of 65 μm^{-1} was previously determined by BET and electrochemistry.[4,26]

Prior to electrochemical experiments, commercial 2D-ITO electrodes were cleaned by successive sonication for 15 min in dichloromethane and acetone. GLAD-ITO electrodes were chemically cleaned by successive soaking for 20 min at 50°C in trichloroethylene, acetone and ethanol. After cleaning, a rectangular section was delimited with nail vanish to define a working electrode area of 0.45 ± 0.05 cm^2. For each electrode, the geometric surface area was used when required in calculations.

Electrochemistry. Cyclic voltammetry was carried out with a PGSTAT-12 Autolab potentiostat (Eco-Chemie) interfaced with GPES-4 software. The counter electrode was a platinum wire, and the reference electrode was either a saturated calomel electrode (isolated from the solution by a salt bridge during electrografting experiments) or Ag/AgCl (Driref-2, WPI Instruments, 0.2 V *vs.* NHE). All electrochemical experiments were performed in a thermostated electrochemical cell.

Electrode functionalization. Electrodeposition was performed on cleaned 2D-ITO and GLAD-ITO electrodes in acidic aqueous solution (10 mL of 20 mM HCl). The 4-diazoniumbenzoic acid was generated *in situ* by mixing 5 mM 4-aminobenzoic acid with 5 mM $NaNO_2$ for 20 min at 4°C under argon. The temperature was maintained at 4°C with a circulating glycerol/ethanol bath, and electrodeposition was achieved by cycling the electrode between 0.5 and -0.8 V *vs* SCE at 0.1 $V \cdot s^{-1}$. The resulting functionalized electrodes were carefully rinsed with purified water.

Immobilization of Fc-NH_2 (or TAPP) was achieved by depositing a drop (50 µL) of solution containing 50 mM EDC, 500 µM Fc-NH_2 (or TAPP) and 0.1 M MES buffer (pH 5.5) onto a pre-functionalized working electrode area. The drop was left in contact for 3 hours at room temperature. Immobilization of rN6KHbI was achieved in two steps. First, activation of the immobilized carboxylates was achieved by depositing a drop (50 µL) of solution containing 25 mM EDC, 25 mM NHS and 0.1 M MES buffer (pH 5.5) onto a pre-functionalized working electrode area. The drop was left in contact for 1.5 hours at room temperature. The electrodes were then rinsed with purified water, and a second drop (50 µL) containing 50 µM of rN6KHbI in a 0.1 M HEPES buffer (pH 7.5) was deposited and held on the electrode for 1 hour at room temperature. In all cases, special care was taken to avoid drop evaporation by keeping the electrode in a humid environment within a covered Petri dish. Negative controls were systematically prepared using the same procedure but in the absence of EDC. The resulting modified electrodes were then rinsed abundantly with purified water and immersed in electrolyte solution (0.1 M HEPES + 0.3 M KCl, pH 7.5) prior to characterization. For the long-term desorption kinetics studies, the modified electrodes were maintained at 4°C in the electrolyte solution.

rN6KHbI expression and purification. The expression and purification of $(Lys)_6$-tagged recombinant rN6KHbI are described in the ESI. The affinity of rN6KHbI for H_2S was determined previously,[23] and found to be similar to that of the tag-free protein rHbI (k'_{on}= 8.7 (± 0.1)×10^4 $M^{-1}\cdot s^{-1}$, k_{off} = 6.7 (± 2.2)×10^{-3} s^{-1} and K'_d= 340 nM for rN6KHbI , k'_{on}= 7.5 (± 0.7)×10^4 $M^{-1}\cdot s^{-1}$, k_{off} = 7.5 (± 2.5)×10^{-3} s^{-1} and K'_d= 378 nM for rHbI).

UV-visible absorption spectroscopy. UV-visible absorption spectra were recorded in a quartz cell (1 cm-path length) using a TORUS UV-visible spectrophotometer (Ocean Optics), and a

balanced deuterium tungsten light source (Micropack). After subtraction of the blank GLAD-ITO contribution, surface coverages (Γ in mol·cm^{-2}) of immobilized TAPP and rN6KHbI were calculated from the spectra according to equation 1:

$$\Gamma = \frac{A_{Soret} - A_{\lambda}}{1000 \times (\varepsilon_{Soret} - \varepsilon_{\lambda})} \quad (1)$$

This equation takes into account the difference between the maximal Soret band absorbance (at 432 nm and 407 nm for TAPP and rN6KHbI, respectively) and the absorbance at λ = 510 nm (for TAPP) or 460 nm (for rN6KHbI). The extinction coefficients determined for the soluble species were: for TAPP in DMF, ε_{Soret} = 178 000 M^{-1}·cm^{-1} and ε_{510} = 12 000 M^{-1}·cm^{-1}, and for rN6KHbI in HEPES at pH 7.5, ε_{Soret} = 178 000 M^{-1}·cm^{-1} and ε_{460} = 5 000 M^{-1}·cm^{-1}.

Titration of H_2S into rN6KHbI. Quartz cuvettes were pre-filled with 2 mL of 0.1 M HEPES at pH 7.5, and a 2 µm-thick GLAD-ITO/rN6KHbI electrode was positioned within the cuvette and perpendicular to optical path. Na_2S solutions were freshly prepared in HEPES buffer (0.1 M, pH 7.5) immediately before use. 2 µL aliquots of 1 mM or 10 mM Na_2S were successively added to the cuvette, and optical measurements were performed 30 s after each H_2S addition. The limit of detection was defined as the lowest concentration allowing to decipher the signal from 2-times the standard deviation of the electrode absorbance in absence of detectable amounts of H_2S (i.e. for $[S]_{tot}$ < 0.3 µM).

3. Results and Discussion

Electrode pre-functionalization. Flat 2D-ITO and 1 µm-thick GLAD-ITO electrodes were electrochemically functionalized with 4-diazoniumbenzoic acid salt generated *in-situ* through cyclic voltammetry (CV) scans performed at 0.1 V·s^{-1}. During the first CV scan, an intense and irreversible cathodic peak was observed at -0.47 V *vs* SCE on both electrodes (Figure S1), which

is characteristic of the one-electron reduction of the aryl-diazonium salt leading to the formation of the aryl radical. The amount of aryl radical generated at the surface of the electrodes can be roughly estimated by integrating the irreversible faradaic peak. After the first CV cycle, a charge equivalent to the reduction of ~4 nmol·cm^{-2} of the diazonium salt is obtained at the 2D-ITO electrode, whereas charge equivalent to ~66 nmol·cm^{-2} was observed at the GLAD-ITO electrode. The much higher value obtained at the GLAD-ITO electrode is mainly attributed to convection-assisted mass transport in solution, allowing for a larger amount of aryl-diazonium to reach the electrode. Despite this, the charge passed was only 16-fold larger than at the 2D-ITO electrode whereas the surface area enhancement of the GLAD electrode is estimated to be ~65.[26] It is thus expected that after 1 CV cycle, the electrografted film density is much lower on a GLAD-ITO electrode than on a 2D-ITO electrode. This assertion is corroborated by the second CV cycle which shows a strongly decreased irreversible peak at the 2D-ITO electrode (the charge passed corresponds to only 15% of that calculated during the first cycle), while it is only slightly decreased at the GLAD-ITO electrode (the charge passed during the second cycle remains high and is equivalent to the formation of 48 nmol·cm^{-2} aryl radicals).

After 10 consecutive CV cycles performed at the GLAD-ITO electrode, the cumulated charge is equivalent to the reduction of ~ 280 nmol·cm^{-2} diazonium salt, which is 70 times more than the charge passed during the first CV cycle at the 2D-ITO electrode. According to the 65-fold surface enhancement of 1 μm-thick GLAD-ITO electrodes, and assuming similar yields for the grafting reaction, this would lead to an electrografted film of similar density to that obtained after one CV cycle at a 2D-ITO electrode. Once the electrografting process is complete, the 2D-ITO and GLAD-ITO electrode surfaces (denoted “PA/2D-ITO” and “PA/GLAD-ITO”, respectively) are covered with a strongly-anchored phenylacetic acid (PA) layer that can then be used for

further functionalization with Fc-NH_2, TAPP or rN6KHbI through amide bond coupling (see experimental section for details).

Electrochemical characterization of amidoferrocene-modified electrodes. Fc-NHCO-/2D-ITO and Fc-NHCO-/GLAD-ITO electrodes and their corresponding negative control electrodes were soaked for 2-3 hours in buffered electrolyte solution prior to characterization to allow desorption of the poorly physisorbed fraction of amidoferrocene. For the negative control electrodes (prepared in the absence of EDC), no faradaic current component could be detected by CV, which demonstrates the absence of ferrocene on the PA-modified surface. *On contrario*, for 2D-ITO and GLAD-ITO modified electrodes prepared in the presence of EDC, CVs (Figure 1) exhibit well-defined, symmetrical peaks centered at 278 and 213 mV *vs.* Ag/AgCl, respectively. The faradaic current intensity also varies linearly with the scan rate in the range 10 - 100 $mV \cdot s^{-1}$. The peaks can be attributed to the reversible one-electron oxidation of the covalently immobilized amidoferrocene moiety.

Surface coverage of the immobilized amidoferrocene was estimated from integration of the faradaic peaks assuming a one-electron redox process. From the data presented in Figure 1, the Fc-NHCO- surface coverage Γ (*i.e.* normalized to the geometric electrode area) at the 1 µm-thick GLAD-ITO electrode is 5800 $pmol \cdot cm^{-2}$, which is 50 times higher than that obtained at the planar ITO electrode (Γ_{2D}= 114 $pmol \cdot cm^{-2}$). This corresponds to ~20% and 25% surface saturation for the 2D-ITO and GLAD-ITO electrodes, respectively, assuming a saturated surface coverage of 450 $pmol \cdot cm^{-2}$ for a close-packed monolayer of Fc (modelling Fc as 7 Å diameter rigid spheres).[27].

The large anodic shift of the formal potential of Fc^+/Fc recorded at the modified electrodes as compared to that of Fc-NH_2 in solution (E^0 = - 65 mV *vs.* Ag/AgCl, see Figure 1) is fully

consistent with the formation of a covalent amide bond between the carboxylate layer and the aminoferrocene. Also, as usually reported for other Fc-NHCO- or Fc-CONH-modified electrodes (see Table S1), the peak separation and FWHM values deviate significantly from the values expected for an ideal Nernstian reversible one-electron transfer with independent immobilized redox probes (i.e. 0 and 90 mV, respectively).[28] This is generally assumed to arise from interactions between neighboring immobilized ferrocene molecules, which results in a broadening of the faradaic waves for surface coverages greater than 20%.[27,29,30] Some heterogeneity in the local microenvironment of the immobilized redox probe could also be responsible for dispersion of both the formal potential,[31,32] and the interfacial electron rate constant.[33] Upon increasing the scan rate, the peak potential separation starts increasing for $\nu >$ 0.2 V s^{-1} (Figure 1C), indicating a progressive shift toward kinetic control by interfacial electron transfer.[28] The data were fitted to the theoretical peak potential calculated with the classical Butler-Volmer equations for a surface-confined redox reaction. Assuming a charge transfer coefficient α of 0.5, the heterogeneous electron transfer rate constant was estimated to be 40 s^{-1} for both electrode types. The fact that similar rate constants were obtained for planar and mesoporous Fc-NHCO- functionalized electrodes further suggests that they have intermediate carboxylate multilayers characterized by similar chemical compositions and densities.

Characterization of the TAPP- and rN6KHbI-modified electrodes by UV-visible absorption spectroscopy. PA/GLAD-ITO modified with TAPP or rN6KHbI (see experimental section for details) were characterized by UV-visible absorption spectroscopy, taking advantage of the strong absorbance of the heme moiety. The spectra obtained after subtraction of the unmodified GLAD-ITO blank are given in Figure 2 and compared to the spectra recorded for TAPP or rN6KHbI in homogeneous solution. In the case of immobilized TAPP, a sharp Soret

band is observed at 432 nm. This Soret band is sharper and blue-shifted as compared to the corresponding band for TAPP solubilized in a neutral aqueous buffer solution, but close to that obtained for TAPP solubilized in DMF. We assume that the spectroscopic features obtained for the soluble porphyrin are indicative of aggregation due to the moderate solubility of TAPP in aqueous solution, wherein the red-shift of the Soret band possibly indicates some J-aggregation.[34] In contrast, the sharp Soret band observed for the modified electrode is evidence for independent TAPP units.

In the case of rN6KHbI, the spectroscopic features of the soluble and immobilized protein are identical, showing a sharp Soret band centered at 407 nm, typical of the high-spin met-aquo form. This indicates that no significant denaturation of the protein occurs during the immobilization process, which is further confirmed below based on reactivity with H_2S. Attempts to draw further insights into the heme conformation of the immobilized protein by resonance Raman spectroscopy were, however, unsuccessful. This is attributed to a strong fluorescence background arising from the electografted layer that prevents reliable detection of the immobilized protein (see Figure S2). This complication is specific to the two-step immobilization strategy used in the present work, because the strong fluorescence background was not observed for modified GLAD-ITO electrodes prepared by simple physisorption of hemoproteins directly at the metal oxide surface.[32]

For each of the modified electrodes, the surface coverage of immobilized molecules was inferred from the absorbance of the Soret band (see experimental section and equation 1). From the data of Figure 2, surface coverages of 610 $pmol \cdot cm^{-2}$ were found for both TAPP and rN6KHbI. In the case of rN6KHbI, reproducibility of the surface functionalization procedure was

attested by the low standard deviation determined from 5 different 1 µm-thick rN6KHbI GLAD-ITO electrodes, leading to an average Γ_0 value of 611 ± 50 pmol·cm^{-2}.

It is worth noting that attempts were made to characterize the rN6KHbI/GLAD-ITO electrodes by UV-visible absorption spectroelectrochemistry, but in contrast to our previous results with cytochrome c or neuroglobin-modified GLAD-ITO electrodes,[6] it was not possible to electrochemically reduce the immobilized protein by applying a cathodic potential. This result was attributed to the lack of direct electronic communication between the heme and the underlying conductive surface.

Stability of the modified electrodes under hydrolytic conditions. In order to analyze the stability of the modified GLAD-ITO electrodes, the surface coverage of immobilized molecules was measured while the modified electrode was soaked in pure electrolyte solution. For such analysis, the initial surface coverage was estimated directly after the post-modification rinsing step. The experimental data obtained are given in Figure 3 (A, B). For each of the three electrodes, a bi-phasic time-course surface coverage decrease was observed, indicative of two separate fractions of adsorbed molecules characterized by different stability. The experimental data were thus fitted to the following bi-exponential decay function (2):

$$\Gamma = \Gamma_{\varphi} e^{-k_{\varphi} t} + \Gamma_{\chi} e^{-k_{\chi} t} \qquad (2)$$

where Γ_{φ} and Γ_{χ} correspond to the less stable and more stable fractions of immobilized molecules, respectively. The resulting fitting parameters are given in Table 1. In the case of rN6KHbI, the surface coverage of the negative control follows a simple monoexponential decay function (see Figure 3) from which the kinetic parameter reported in Table 1 has been recovered. For all modified electrodes, a highly stable fraction Γ_{χ} of immobilized molecules is observed despite the high ionic strength (I = 0.45 M) and hydrolytic conditions used in the experiment. A

significant quantity of immobilized molecules is still detected even after a few days immersion in the electrolyte solution at 4°C. This amount corresponds to a surface coverage of 4350 pmol·cm^{-2} of Fc-NHCO after 6 days (*i.e.* 75% of Γ_χ), 605 pmol·cm^{-2} of TAPP after 12 days (*i.e.* 92% of Γ_χ), and 477 pmol·cm^{-2} of rN6KHbI after 20 days (i.e. 45% of Γ_χ). Moreover, in the absence of EDC, neither Fc-NH_2 nor TAPP are detected in the corresponding negative control experiments, which is not the case for rN6KHbI where a significant amount is observed. The latter result is evidence for the formation of a physisorbed rN6KHbI fraction that completely desorbs within 24 hours (see Figure 3B). These observations demonstrate that the more-stable Γ_χ fraction results from the formation of a stable covalent bond between the coupled molecule and the electrografted carboxylate layer once activated by EDC. They also confirm that the diazonium-electrografting strategy is a viable approach to functionalizing ITO surfaces with stable and highly robust molecular layers.[11–13]

It should be noted, however, that the Γ_χ value is strongly dependent on the nature of the immobilized molecule. In the case of Fc-NHCO, Γ_χ is equivalent to ~13 saturated monolayers of Fc-NH_2 on a planar electrode, which, once compared to the ~65 surface enhancement of the 1 μm-thick nanostructured GLAD-ITO film, leads to the conclusion that only 20% of a saturated monolayer is covering the three-dimensional surface. In the case of TAPP, the stable fraction is equivalent to 2 saturated monolayers (calculated assuming the porphyrin ring is perpendicular to the grafting surface), a value which remains low in comparison to the surface enhancement of the GLAD-ITO film. And finally, in the case of rN6KHbI, Γ_χ is equivalent to ~ 30 saturated monolayers, assuming a saturating surface coverage of Γ_{2D} = 20 pmol·cm^{-2} for rN6KHbI (by analogy to cytochrome c that is of similar size).[6] The highly stable protein fraction immobilized at the 1 μm-thick rN6KHbI/GLAD-ITO electrode thus corresponds to ca. 45% of a

saturated protein monolayer, which is a high value. Accordingly, the efficiency of the EDC coupling reaction is higher for rN6KHbI than for Fc-NH_2 and TAPP. This result can be attributed to the affinity of the positively charged rN6KHbI (pI estimated to be 9.7) for the negatively charged PA/GLAD-ITO electrode, which leads to pre-concentration of the protein within the mesoporous structure of ITO and favorable chemical coupling inside the porous electrode. This electrostatic contribution is in agreement with the physisorbed rN6KHbI detected at the negative control electrode, as discussed above. Moreover, the slow desorption of rN6KHbI ($t_{1/2}$ ~ 4 h) in a high ionic strength electrolyte (I = 0.45 M) attests to strong electrostatic interactions between rN6KHbI and the electrografted carboxylate layer.

In the case of Fc-NH_2, it is surprising that a significant fraction Γ_φ of immobilized ferrocene desorbs rapidly, yet is still characterized by a formal oxidation potential value representative of a Fc-NHCO species coupled to a benzoyl group. This result can be interpreted by assuming that during the electrografting pre-functionalization step, a significant amount of carboxylic acid-bearing organic compounds remains physically entrapped within the electrografted layer, even after thorough rinsing. During covalent coupling, these entrapped molecules could react with the small Fc-NH_2 molecule. It is only upon soaking the electrode in a high ionic strength buffer and applying an oxidizing potential that these physisorbed amidoferrocene compounds would progressively desorb.

Influence of the GLAD ITO film thickness. The complete functionalization process described above on 1 μm-thick GLAD-ITO electrodes was also used to modify GLAD-ITO electrodes characterized by various film thicknesses in the range 0.3 to 2 μm (see Figure S3 for SEM images). Concerning the main growth scaling parameters of such GLAD mesoporous films, it was previously shown by both BET and electrochemistry, that the surface enhancement of the

GLAD films varies linearly with the film thickness.[4,26] *On contrario*, the mean-rod diameter, void spacing and center-to-center spacing follow a power law with an exponential factor between 0.3 and 0.5. From analysis of top-view SEM images of GLAD-ITO films, the center-to-center spacing was thus found to vary from *ca* 40 nm at 250 nm to *ca* 90 nm at 2 μm. These values are much larger than the molecular probes used in the present study (modelled as spheres with diameters of ca. 7 Å for Fc-NH_2 and 5 nm for rN6KHbI), so that accessibility of the entire film surface should not be limited by steric considerations.

The resulting Fc-NHCO/GLAD-ITO and rN6KHbI/GLAD-ITO electrodes were characterized by electrochemistry and UV-visible absorption spectroscopy, respectively. The surface coverage of the strongly anchored molecules (Γ_χ) was determined after 2-3 h of desorption in the electrolyte solution (to remove the poorly physisorbed fraction, Γ_φ), and plotted as a function of film thickness (Figure 3 C,D). For both electrodes, a near-linear relationship was observed. We moreover investigated the stability of a 2 μm GLAD-ITO/rN6KHbI electrode as a function of the soaking time in electrolyte solution. The experimental data are plotted in Figure 3B and fitted to a bi-exponential decay (see Table 1), giving results similar to those obtained at the 1 μm-thick rN6KHbI/GLAD-ITO electrode.

Collectively, these results demonstrate that the present 2-step functionalization process allows for a rather homogeneous distribution of the grafted molecules throughout the entire mesoporous film thickness, taking full benefit of the surface area enhancement of the GLAD-ITO film.

Application to H_2S biosensing. 2 μm-thick rN6KHbI/GLAD-ITO electrodes were next tested as an optical biosensing platform to detect H_2S in a buffer solution. First, the biosensor was successively soaked in 2 mL of 0.1 M HEPES buffer solutions at pH 7.5 containing 0 or 100 μM Na_2S. The recorded spectra (Figure S4) and difference spectra (Figure 4A) are similar to those

obtained for the soluble protein in a homogenous solution. For both the biosensor and soluble protein, the maximum of the Soret band shifts from 407 to 426 nm when transferred to H_2S solution, while the Soret intensity decreases strongly. This behavior is characteristic of the expected transition from the high-spin His-Fe^{III}-aquo coordination mode to the low-spin His-Fe^{III}-SH_2 coordination mode. The initial surface coverage of the His-Fe^{III}-aquo protein is estimated to be 855 pmol·cm^{-2}, while after addition of a saturating concentration of H_2S the amount of His-Fe^{III}-SH_2 formed is estimated to be 865 pmol·cm^{-2} (*i.e.*, assuming an extinction coefficient difference at 426 nm of $\Delta\varepsilon_{426} = \varepsilon_{426}$ (His-Fe^{III}-aquo) – ε_{426} (His-Fe^{III}-SH_2) = 120200 $M^{-1}.cm^{-1}$). This result indicates that the heme pockets of all immobilized rN6KHb proteins remain accessible to H_2S and reactive. This is also consistent with the sharp and symmetric Soret band obtained under saturated H_2S concentrations (see Figure S4). The process is also reversible, since soaking the electrode in an H_2S-free buffered solution allows recovery of the initial spectrum of the His-aquo state (Figure 4C). Reproducible absorbance changes were recorded after successive dipping of the modified electrode in different buffered solutions containing either 0 μM or 100 μM Na_2S (Figure 4C), demonstrating that the same biosensing electrode can be repeatedly used to monitor increasing as well as decreasing concentrations of H_2S. Furthermore, the spectra that were recorded immediately after soaking the electrode in H_2S solution were observed to reach a steady state absorbance nearly instantaneously, a behaviour which attests of the fast response time of the biosensor (less than a few seconds). This is fully consistent with the fast ligandation/deligandation rates of H_2S at HbI that were recently re-evaluated.[23]

In order to determine the binding affinity of H_2S to the biosensor, spectra were recorded at a 2 μm-thick rN6KHbI/GLAD-ITO electrode immersed in 2 mL of a 0.1 M HEPES buffer solution

(pH 7.5) containing increasing concentrations of H_2S up to a saturated value of 100 μM (see Figure 4A). It should be mentioned here that the pK_a value of the H_2S/HS^-couple is 6.8,[35] so at pH 7.5, the deprotonated HS^- form predominates, whereas the recombinant protein rN6KHbI selectively binds the protonated form H_2S.[22] The absorbance changes were thus plotted as a function of the total sulfur concentration $[S]_{tot} = [H_2S] + [HS^-]$ (see Figure 4B). In order to estimate the apparent affinity constant K_d' of H_2S for the biosensor, the experimental data were fitted to equation 3,

$$\Delta A = A_\lambda - A_{460} = \Delta A_0 - (\Delta\varepsilon_\lambda - \Delta\varepsilon_{460}) \frac{K_d' + x + \frac{\Gamma_0 S}{V} - \sqrt{\left(K_d' + x + \frac{\Gamma_0 S}{V}\right)^2 - 4\frac{\Gamma_0 S}{V}x}}{2\frac{S}{V}} \qquad (3)$$

where x is the total concentration of sulfur in solution, ΔA_0 the initial absorbance difference, $\Delta\varepsilon_\lambda$ the difference in the extinction coefficients of the His-Fe^{III}-aquo and the His-Fe^{III}-SH_2 forms (*i.e.* $\Delta\varepsilon_\lambda = \varepsilon_\lambda$(His-$Fe^{III}$-aquo) - ε_λ(His-Fe^{III}- SH_2)) K_d' the apparent dissociation constant, Γ_0 the initial surface coverage of rN6KHbI (calculated from ΔA_0 according to equation 1), S the geometric surface area of the GLAD-ITO film (i.e. 0.45 cm^{-2}) and V the volume of solution (i.e. 2 cm^3). The experiment was repeated in quadruplicate and an apparent K_d' value of 9.1 ± 4.7 μM was inferred from the non-linear regression fit of equation 3 to the experimental data. This is much higher than the K_d' of 340 nM obtained for rN6KHbI solubilized in a 0.1 M HEPES buffer of pH 7 (a homogeneous binding affinity that corroborates the recent report for the recombinant untagged HbI).[23] The lower affinity we observed for the immobilized protein cannot result from an intrinsically lower affinity due to surface-confinement effects or protein denaturation because the UV-visible features (wavelengths and intensities) of His-Fe^{III}-aquo and His-Fe^{III}-SH_2 of both the immobilized and soluble protein are fully consistent. Rather, we propose that the

functionalized mesoporous ITO film is characterized by a high local ionic strength and an excess of negative charge (due to the large excess of grafted carboxylate groups as compared to the surface coverage of protein) resulting in an unfavourable partition coefficient for both the hydrophobic H_2S and negatively charged HS^-. Assuming that the intrinsic affinity of immobilized rN6KHbI remains unaffected, this would mean that the unfavourable partition coefficient is ~1/30 = 0.033. This strong influence of the local environment on the partition coefficient of small ligands is similar to that previously observed for O_2 at GLAD-ITO electrodes functionalized with microperoxidase-11, where a favourable partition coefficient of 70 was proposed.[26] Despite such an adverse effect, the limit of detection for H_2S is still in the low μM range. From the H_2S titration plots shown in Figure 5, it is possible to estimate the analytical performance of the biosensor. The two plots were obtained from two independent HbI-modified electrodes each functionalized with a distinct protein surface concentration (*i.e.*. 1040 and 390 pmol·cm^{-2}), showing that even though the 2 curves were off-set because of the different amount of HbI, both function within the same dynamic range from 2 to 50 μM $[S]_{tot}$, and have similar limits of detection around 2 ± 0.5 μM $[S]_{tot}$. This detection limit is in reality equivalent to 0.35 ± 0.1 μM H_2S when considering the acid/base equilibrium of $[S]_{tot}$ at pH 7.5.

In order to approach measurements in complex biological fluids, we also challenged the selectivity of our biosensor by investigating the effect of other biologically relevant sulfur compounds in HEPES buffer. In the presence of 1 mM of either cysteine or glutathione, the UV-visible absorption spectrum of the modified rN6KHbI/GLAD-ITO electrode displays a Soret band at 407 nm typical of His-Fe^{III}-aquo coordination, indicating that these two sulfur compounds do not interact with the heme. Interestingly, H_2S titration experiments performed in

the presence of cysteine or glutathione indicate that they do not affect the affinity of the biosensor for its target analyte (data not shown).

Finally, we demonstrated that the biosensor is able to detect hydrogen sulfide in human plasma, a complex medium containing around 0.1 M of chloride along with a wide range of proteins (*e.g.* 500 µM of serum albumin) and other small molecules. Titration experiments carried out in two plasma samples from two different healthy donors afforded K'_d values of 4.8 and 6.2 µM. These values are close to that reported above in a pure HEPES buffer, again highlighting the absence of biological matrix effects on the analytical response of the optical biosensor.

Overall, the rN6KHbI-modified GLAD-ITO film is the first example of an H_2S biosensor whose inherent characteristics are compatible with use in biological samples. As compared to electrochemical biosensors based on the ability of H_2S to inhibit various peroxidases,[21] it has two main advantages. The first is that, in contrast to the peroxidase method, the optical sensor does not require the addition of any extra reagents to the sample, which could interfere with the analysis. The second is that the optical biosensing approach can be used as an absolute quantitative analytical method to determine H_2S concentration, without the need for calibration. This is made possible by the fact that before each measurement, we can accurately determine by UV-visible absorption spectroscopy the amount of bioreceptor present on the biosensing surface (*i.e.*, Γ_0). Knowing the affinity binding constant K_d' and using equation 3, this allows an immediate quantification of H_2S concentration (such as performed in Figure 5). Although the limit of detection of the present biosensor is clearly not competitive with MS/MS-liquid chromatography[36] or some fluorescent probes (LOD ~ 10 nM),[37] it does however allow for fast and reversible detection that none of these alternate techniques are capable of.

4. Conclusion

In this study, we demonstrate that the combination of a preliminary electrochemical grafting step followed by a chemical coupling reaction is a versatile 2-step functionalization method allowing for reproducible immobilization of large amounts of functional (bio)molecules homogeneously distributed within transparent high surface area mesoporous metal oxide electrodes. The modified electrodes resist high ionic strength hydrolytic conditions and can be quantitatively characterized using a variety of analytical techniques such as electrochemistry or UV-visible absorption spectroscopy. In a proof of concept, we establish that these modified electrodes can be used as biosensors for analytical purposes in both model environments as well as more complex biological samples. This study paves the way for the development of innovative opto-electrochemical biosensors in which the use of coupled detection methods would offer a significant gain in selectivity and/or sensitivity.

Acknowledgments

V.B. thanks Stéphanie Lau-Truong (ITODYS) for assistance in Raman spectroscopy. K.D.H. thanks Jeremy Sit for ongoing access to the GLAD evaporator, Jae-Young Cho for SEM microscopy, and the NRC Nanotechnology Initiative GIANNT project for partial funding support.

REFERENCES

[1] M. Mierzwa, E. Lamouroux, A. Walcarius, M. Etienne, Porous and Transparent Metal-oxide Electrodes : Preparation Methods and Electroanalytical Application Prospects, Electroanalysis. 30 (2018) 1241–1258. doi:10.1002/elan.201800020.

[2] P.R. Solanki, A. Kaushik, V. V. Agrawal, B.D. Malhotra, Nanostructured metal oxide-based biosensors, NPG Asia Mater. 3 (2011) 17–24. doi:10.1038/asiamat.2010.137.

[3] M.J. Brett, M.M. Hawkeye, New materials at a glance, Science (80-.). 319 (2008) 1192–1193. doi:10.1126/science.1153910.

[4] K.M. Krause, M.T. Taschuk, K.D. Harris, D.A. Rider, N.G. Wakefield, J.C. Sit, J.M. Buriak, M. Thommes, M.J. Brett, Surface area characterization of obliquely deposited metal oxide nanostructured thin films., Langmuir. 26 (2010) 4368–76. doi:10.1021/la903444e.

[5] C. Renault, K.D. Harris, M.J. Brett, V. Balland, B. Limoges, Time-resolved UV-visible spectroelectrochemistry using transparent 3D-mesoporous nanocrystalline ITO electrodes, Chem. Commun. 47 (2011) 1863–1865. doi:10.1039/C0CC04154H.

[6] D. Schaming, C. Renault, R.T. Tucker, S. Lau-Truong, J. Aubard, M.J. Brett, V. Balland, B. Limoges, Spectroelectrochemical characterization of small hemoproteins adsorbed within nanostructured mesoporous ITO electrodes., Langmuir. 28 (2012) 14065–72. doi:10.1021/la302913j.

[7] M. Kato, T. Cardona, A.W. Rutherford, E. Reisner, Covalent Immobilization of Oriented Photosystem II on a Nanostructured Electrode for Solar Water Oxidation, J. Am. Chem. Soc. 135 (2013) 10610–10613. doi:10.1021/ja404699h.

[8] V. Müller, J. Rathousky, D. Fattakhova-Rohlfing, Covalent immobilization of redox protein within the mesopores of transparent conducting electrodes, Electrochim. Acta. 116 (2014) 1–8. doi:10.1016/j.electacta.2013.10.136.

[9] E. González-Arribas, T. Bobrowski, C. Di Bari, K. Sliozberg, R. Ludwig, M.D. Toscano,

A.L. De Lacey, M. Pita, W. Schuhmann, S. Shleev, Transparent, mediator- and membrane-free enzymatic fuel cell based on nanostructured chemically modified indium tin oxide electrodes, Biosens. Bioelectron. 97 (2017) 46–52. doi:10.1016/j.bios.2017.05.040.

[10] D. Lin, K.D. Harris, N.W.C. Chan, A.B. Jemere, Nanostructured indium tin oxide electrodes immobilized with toll-like receptor proteins for label-free electrochemical detection of pathogen markers, Sensors Actuators, B Chem. 257 (2018) 324–330. doi:10.1016/j.snb.2017.10.140.

[11] R. Bangle, R.N. Sampaio, L. Troian-Gautier, G.J. Meyer, Surface Grafting of Ru(II) Diazonium-Based Sensitizers on Metal Oxides Enhances Alkaline Stability for Solar Energy Conversion, ACS Appl. Mater. Interfaces. 10 (2018) 3121–3132. doi:10.1021/acsami.7b16641.

[12] T.G.A.A. Harris, R. Götz, P. Wrzolek, V. Davis, C.E. Knapp, K. Ly, P. Hildebrandt, M. Schwalbe, I. Weidinger, I. Zebger, A. Fischer, Robust electrografted interfaces on metal oxides for electrocatalysis-an in situ spectroelectrochemical study, J. Mater. Chem. A. 6 (2018) 15200–15212. doi:10.1039/c8ta02983k.

[13] Y.S. Kim, S. Fournier, S. Lau-Truong, P. Decorse, C.H. Devillers, D. Lucas, K.D. Harris, B. Limoges, V. Balland, Introducing Molecular Functionalities within High Surface Area Nanostructured ITO Electrodes through Diazonium Electrografting, ChemElectroChem. 5 (2018) 1625–1630. doi:10.1002/celc.201800418.

[14] C. Bourdillon, M. Delamar, C. Demaille, R. Hitmi, J. Moiroux, J. Pinson, Immobilization of glucose oxidase on a carbon surface derivatized by electrochemical reduction of diazonium salts, J. Electroanal. Chem. 336 (1992) 113–123. doi:10.1016/0022-0728(92)80266-7.

[15] G. Liu, T. Böcking, J.J. Gooding, Diazonium salts: Stable monolayers on gold electrodes for sensing applications, J. Electroanal. Chem. 600 (2007) 335–344. doi:10.1016/j.jelechem.2006.09.012.

[16] M. Pellissier, F. Barrière, A.J. Downard, D. Leech, Improved stability of redox enzyme layers on glassy carbon electrodes via covalent grafting, Electrochem. Commun. 10 (2008) 835–838. doi:10.1016/j.elecom.2008.03.010.

[17] M.A. Booth, K. Kannappan, A. Hosseini, A. Partridge, In-Depth Electrochemical Investigation of Surface Attachment Chemistry via Carbodiimide Coupling, Langmuir. 31 (2015) 8033–8041. doi:10.1021/acs.langmuir.5b01863.

[18] L. Li, P. Rose, P.K. Moore, Hydrogen Sulfide and Cell Signaling, Annu. Rev. Pharmacol. Toxicol. 51 (2011) 169–187. doi:10.1146/annurev-pharmtox-010510-100505.

[19] J.L. Wallace, R. Wang, Hydrogen sulfide-based therapeutics: exploiting a unique but ubiquitous gasotransmitter., Nat. Rev. Drug Discov. 14 (2015) 329–345. doi:10.1038/nrd4433.

[20] S. Rajpal, P. Katikaneni, M. Deshotels, S. Pardue, J. Glawe, X. Shen, N. Akkus, K. Modi, R. Bhandari, P. Dominic, P. Reddy, G.K. Kolluru, C.G. Kevil, Total sulfane sulfur bioavailability reflects ethnic and gender disparities in cardiovascular disease, Redox Biol. 15 (2018) 480–489. doi:10.1016/j.redox.2018.01.007.

[21] T. Xu, N. Scafa, L.-P. Xu, S. Zhou, K. Abdullah Al-Ghanem, S. Mahboob, B. Fugetsu, X. Zhang, Electrochemical hydrogen sulfide biosensors, Analyst. 141 (2016) 1185–1195. doi:10.1039/C5AN02208H.

[22] D.W. Kraus, J.B. Wittenberg, Hemoglobins of the Lucina pectinata / Bacteria Symbiosis, J. Biol. Chem. 265 (1990) 16043–16053.

[23] M. Dulac, A. Melet, E. Galardon, Reversible Detection and Quantification of Hydrogen Sulfide by Fluorescence Using the Hemoglobin I from Lucina pectinata, ACS Sensors. 3 (2018) 2138–2144. doi:10.1021/acssensors.8b00701.

[24] D.W. Kraus, J.B. Wittenberg, L. Jing-Fen, J. Peisach, Hemoglobins of the Lucina pectinata / Bacteria Symbiosis, J. Biol. Chem. 265 (1990) 16043–16053.

[25] C. Ramos-Alvarez, B.-K. Yoo, R. Pietri, I. Lamarre, J.-L. Martin, J. Lopez-Garriga, M.

Negrerie, Reactivity and Dynamics of H_2S, NO and O_2 Interacting with Hemoglobins from Lucina pectinata, Biochemistry. (2013) 7007–7021.

[26] C. Renault, C.P. Andrieux, R.T. Tucker, M.J. Brett, V. Balland, B. Limoges, Unraveling the mechanism of catalytic reduction of O_2 by microperoxidase-11 adsorbed within a transparent 3D-nanoporous ITO film., J. Am. Chem. Soc. 134 (2012) 6834–45. doi:10.1021/ja301193s.

[27] C.E.D. Chidsey, C.R. Bertozzi, T.M. Putvinski, A.M. Mujsce, Coadsorption of ferrocene-terminated and unsubstituted alkanethiols on gold: Electroactive self-assembled monolayers, J. Am. Chem. Soc. 112 (1990) 4301–4306. doi:10.1021/ja00167a028.

[28] E. Laviron, General expression of the linear potential sweep voltammogram in the case of diffusionless electrochemical systems, J. Electroanal. Chem. 101 (1979) 19–28. doi:10.1016/S0022-0728(79)80075-3.

[29] E. Laviron, L. Roullier, General expression of the linear potential sweep voltammogram for a surface redox reaction with interactions between the adsorbed molecules. Applications to modified electrodes, J. Electroanal. Chem. 115 (1980) 65–74. doi:10.1016/S0022-0728(80)80496-7.

[30] L.Y.S. Lee, T.C. Sutherland, S. Rucareanu, R.B. Lennox, Ferrocenylalkylthiolates as a Probe of Heterogeneity in Binary Self-Assembled Monolayers on Gold, Langmuir. 22 (2006) 4438–4444. doi:10.1021/la053317r.

[31] S.E. Creager, G.K. Rowe, Solvent and double-layer effects on redox reactions in self-assembled monolayers of ferrocenyl-alkanethiolates on gold, J. Electroanal. Chem. 420 (1997) 291–299. doi:10.1016/S0022-0728(96)04785-7.

[32] V. Balland, S. Lecomte, B. Limoges, Characterization of the Electron Transfer of a Ferrocene Redox Probe and a Histidine-Tagged Hemoprotein Specifically Bound to a Nitrilotriacetic-Terminated Self-Assembled Monolayer, Langmuir. 25 (2009) 6532–6542. doi:10.1021/la900062y.

[33] K. Weber, S.E. Creager, Voltammetry of Redox-Active Groups Irreversibly Adsorbed

onto Electrodes. Treatment Using the Marcus Relation between Rate and Overpotential, Anal. Chem. 66 (1994) 3164–3172. doi:10.1021/ac00091a027.

[34] R. Giovannetti, The Use of Spectrophotometry UV-Vis for the Study of Porphyrins, in: J. Dr. Uddin (Ed.), Macro To Nano Spectrosc., InTech, 2012: pp. 87–109. doi:10.5772/38797.

[35] M.R. Filipovic, J. Zivanovic, B. Alvarez, R. Banerjee, Chemical Biology of H_2S Signaling through Persulfidation, Chem. Rev. 118 (2018) 1253–1337. doi:10.1021/acs.chemrev.7b00205.

[36] B. Tan, S. Jin, J. Sun, Z. Gu, X. Sun, Y. Zhu, K. Huo, Z. Cao, P. Yang, X. Xin, X. Liu, L. Pan, F. Qiu, J. Jiang, Y. Jia, F. Ye, Y. Xie, Y.Z. Zhu, New method for quantification of gasotransmitter hydrogen sulfide in biological matrices by LC-MS/MS, Sci. Rep. 7 (2017) 46278. https://doi.org/10.1038/srep46278.

[37] Z. Guo, G. Chen, G. Zeng, Z. Li, A. Chen, J. Wang, L. Jiang, Fluorescence chemosensors for hydrogen sulfide detection in biological systems, Analyst. 140 (2015) 1772–1786. doi:10.1039/C4AN01909A.

SCHEME AND FIGURE CAPTIONS

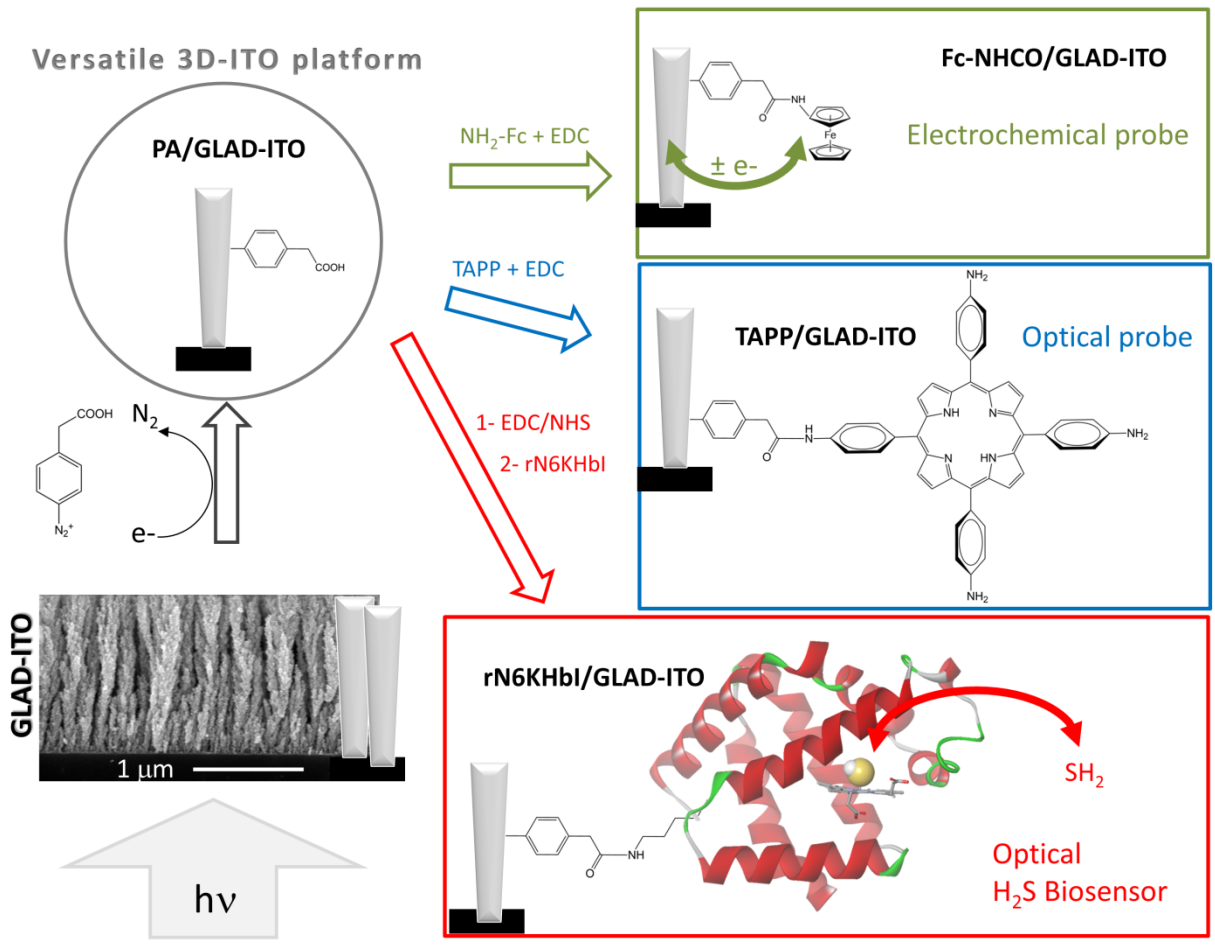

Scheme 1. SEM image of the 1µm-thick GLAD-ITO film, and an illustration of the multistep chemical surface functionalization methodology used in the present work.

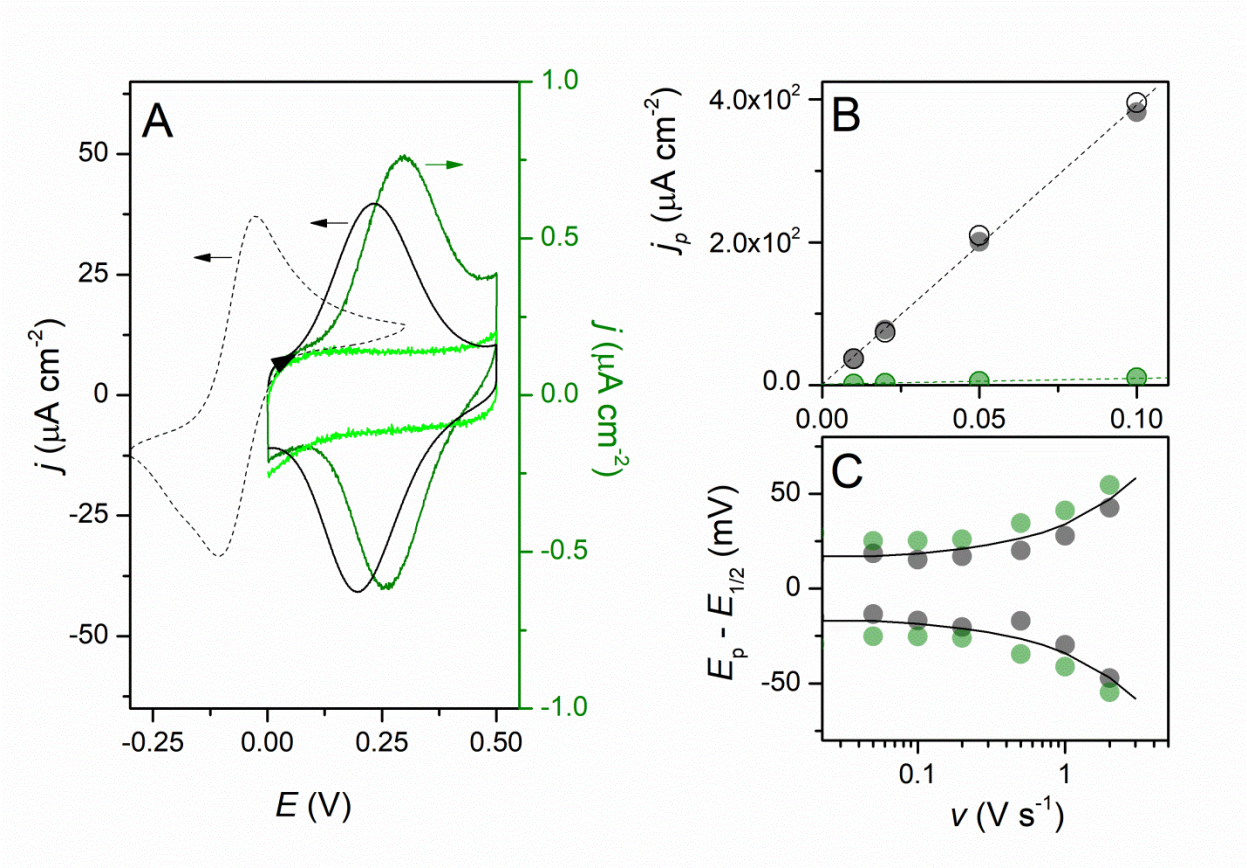

Figure 1. Left: (A) Cyclic voltammograms recorded at (dark green) Fc-NHCO/2D-ITO, (black) 1 μm-thick Fc-NHCO/GLAD-ITO, and (light green) PA/2D-ITO electrodes. The black dashed CV corresponds to Fc-NH_2 in solution (100 μM) recorded at a 2D-ITO working electrode. In all cases, the electrolyte is 0.1M HEPES, 0.3M KCl, pH = 7.5, and the scan rate = 10 mV s^{-1}. Right: Scan rate dependence of the cathodic and anodic peak (B) current densities and (C) potentials for (green) Fc-NHCO/2D-ITO and (black) Fc-NHCO/GLAD-ITO electrodes. *E* is given vs. Ag/AgCl.

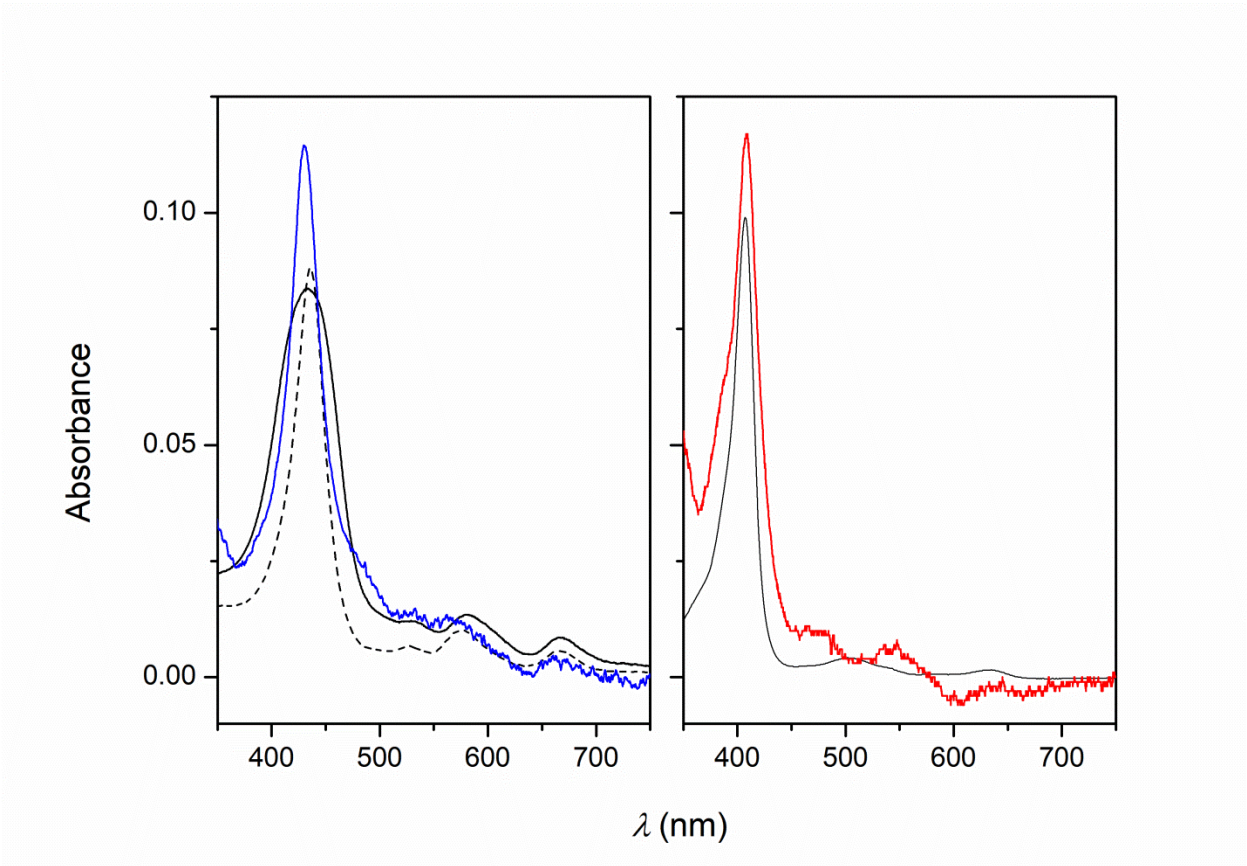

Figure 2. UV-visible absorption spectra of a 1 μm-thick (left, blue) TAPP/GLAD-ITO and (right, red) rN6KHbI/GLAD-ITO electrode after subtraction of the GLAD-ITO contribution. In each plot, spectra for the TAPP and rN6KHbI reagents in solution are also provided for comparison: (left, solid black line) 1 μM TAPP solubilized in a HEPES aqueous buffer at pH 7, (right, solid black) 1 μM rN6KHbI in pH 7 HEPES, and (left, black dashed line) 0.5 μM TAPP solubilized in DMF.

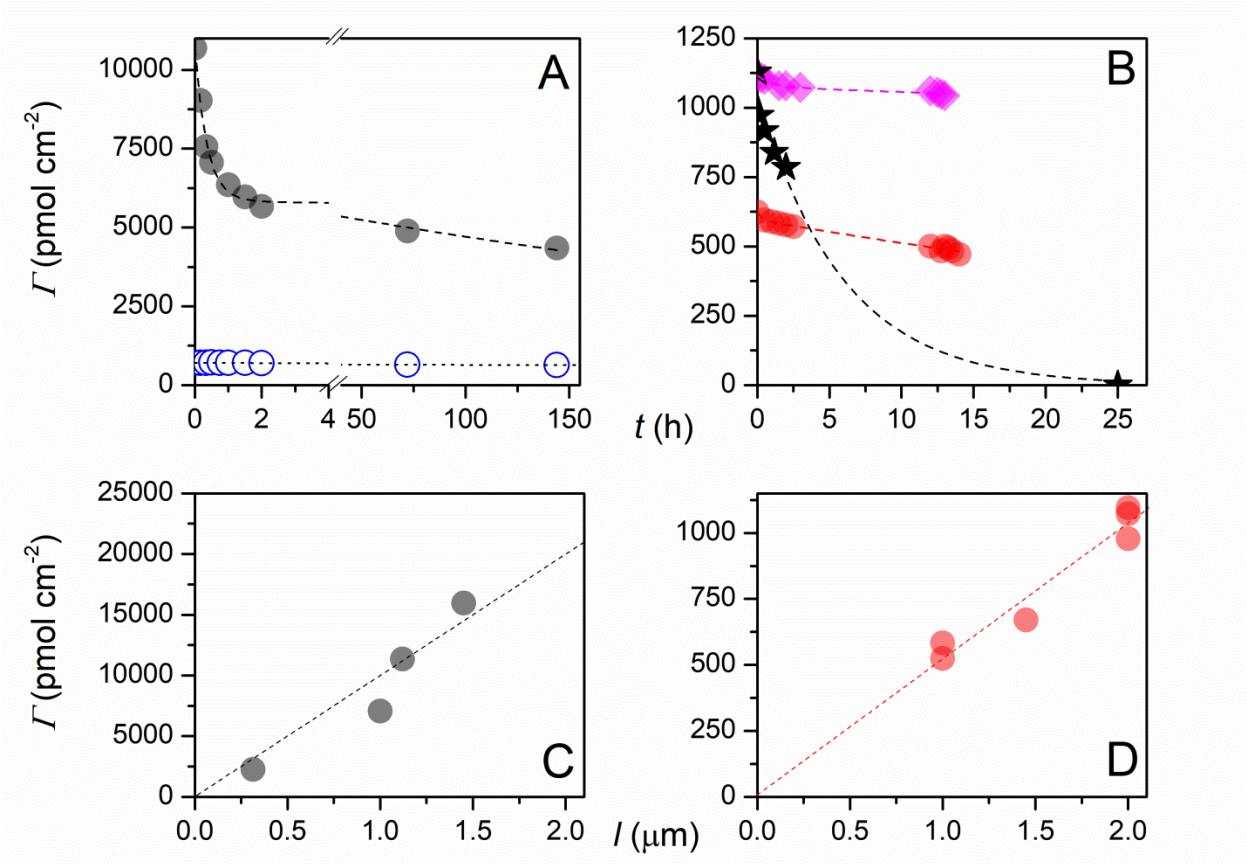

Figure 3. Surface coverage determined at 1 μm-thick functionalized GLAD-ITO electrodes as a function of soaking time in the electrolyte solution for: (A) (●) Fc-NHCO- and (○) TAPP, (B) (●) rN6KHbI. In (B), the coverage data are compared to that obtained at (◆) a 2 μm-thick rN6KHbI/GLAD-ITO electrode and (★) a 1.45 μm-thick GLAD-ITO negative control electrode. All experimental data are fitted to a bi-exponential decay function, except the negative control which is fitted to a mono-exponential decay. (C, D) Surface coverage of (●) Fc-NHCO- and (●) rN6KHbI obtained at functionalized GLAD-ITO electrodes with various film thicknesses *l* after 2-3 hours of soaking in the electrolyte solution. All measurements are performed at 25°C in the electrolyte solution (0.1 M HEPES, 0.3 M KCl, pH 7.5). For long term storage (>few hours), functionalized electrodes are kept at 4°C between each spectroscopic characterization.

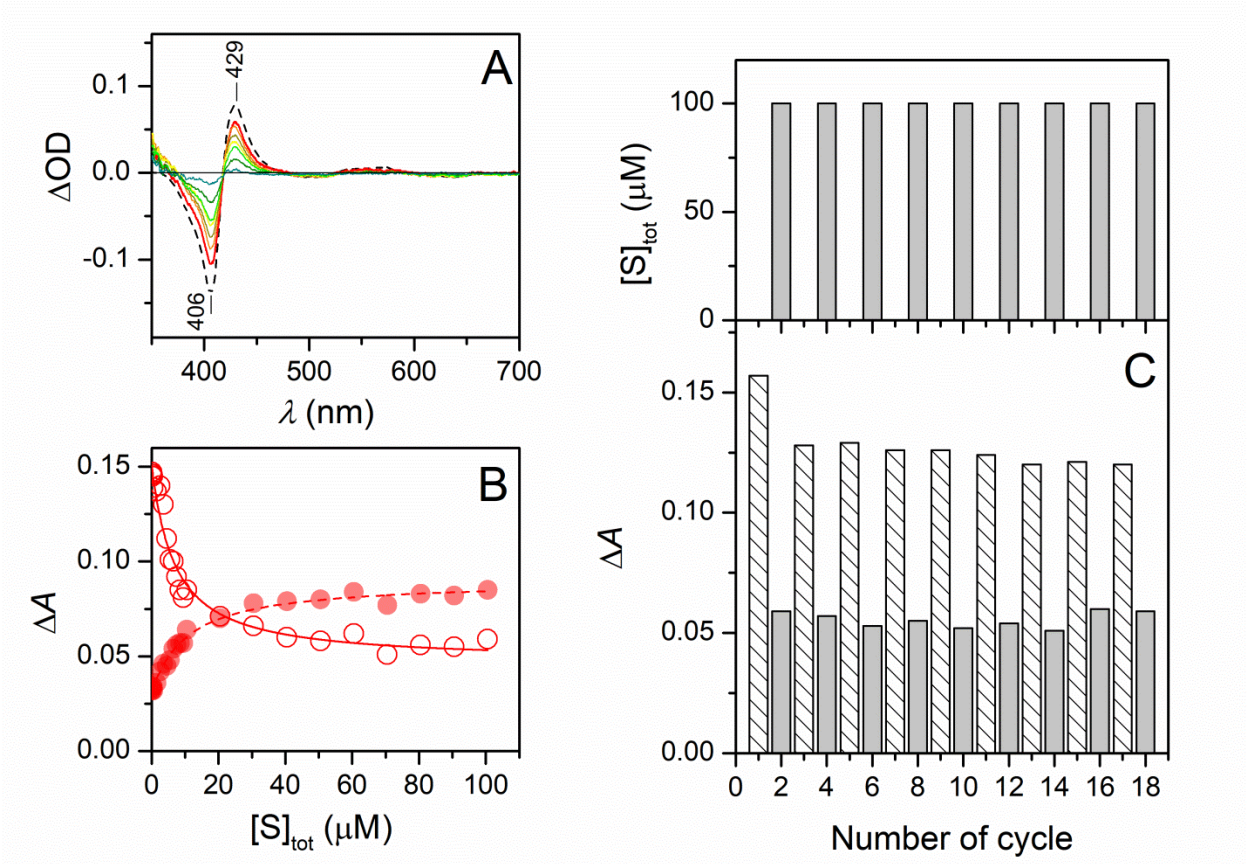

Figure 4. (A) Difference spectra in the absence and presence of increasing concentrations of Na_2S up to 100 μM obtained for (red) a 2 μm-thick rN6KHbI/GLAD-ITO electrode (Γ_0 = 855 pmol·cm^{-2}, S = 0.45 cm^2) and (dashed black) rN6KHbI in solution (ca 1.1 μM); (B) Variation of the 2 μm-thick rN6KHbI/GLAD-ITO electrode absorbance (○) A_{407}-A_{460} and (●) A_{426}-A_{460} as a function of Na_2S concentration in solution. The solid and dashed curves correspond to non-linear regression fits of equation 3 to the experimental data. (C) Absorbance variation (A_{407}-A_{460}) monitored at a 2 μm-thick rN6KHbI/GLAD-ITO electrode soaked successively in buffer solutions containing either (patterned columns) 0 or (grey columns) 100 μM Na_2S. All measurements were performed at 25°C in a 0.1 M HEPES buffer solution at pH 7.5.

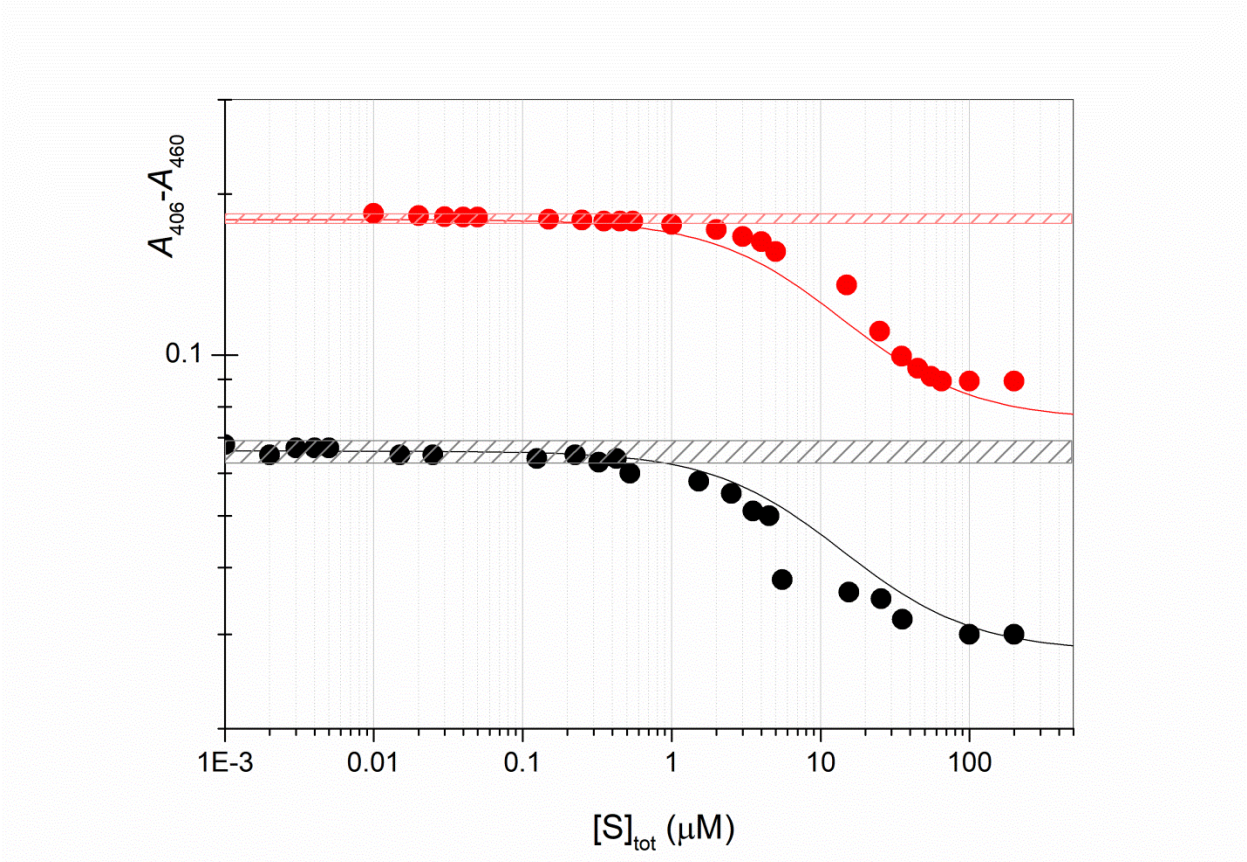

Figure 5. H_2S titration curves obtained from the variation of the absorbance difference ΔA at two independent rN6KHbI/Glad-ITO electrodes characterized by the highest and lowest amount of immobilized protein, *i.e.* (red) Γ_0 = 1 040 and (black) 390 pmol·cm^{-2}. The black and red lines correspond to equation 3 plotted for each electrode by taking into account their specific Γ_0 value and common average values of K_d' =9.1 μM and ($\Delta\varepsilon_{407}$-$\Delta\varepsilon_{460}$) =10^5 M^{-1}·cm^{-1}. The red and black dashed area correspond to the average absorbance value of the electrode ± 2-times the corresponding standard deviation determined in absence of detectable amounts of H_2S. All measurements were performed at 25°C in a 0.1 M HEPES buffer solution at pH 7.5.

Table 1. Surface coverages (pmol·cm^{-2}) and desorption rates (in h^{-1}) of the physisorbed (Γ_φ) and chemisorbed (Γ_χ) fractions identified at mesoporous GLAD-ITO electrodes (film length l) either functionalized in the presence (+) or absence (-) of the coupling reagent EDC.

	l (μm)	EDC	Γ_φ	k_φ	Γ_χ	k_χ
Fc-NHCO-	1	+	4 900	2.7	5 800	21 10^{-3}
TAPP	1	+	50	0.2	660	0.3 10^{-3}
rN6KHbI	1	+	30	3.8	595	15 10^{-3}
rN6KHbI	2	+	40	0.8	1 075	2.5 10^{-3}
rN6KHbI	1.45	-	1 050	0.17	-	-